LASER INTERFEROMETER GRAVITATIONAL WAVE OBSERVATORY
- LIGO -
CALIFORNIA INSTITUTE OF TECHNOLOGY
MASSACHUSETTS INSTITUTE OF TECHNOLOGY

Technical Report LIGO-T990027-00-D 03/12/99

Characterization of the temporal filtering of the BSC to a magnetic field

Serge Lefranc
Universite de Versailles St Quentin-en-Yvelines, FRANCE.

Distribution of this technical report:

LIGO science team

This is an internal working note
of the LIGO Project.

California Institute of Technology
LIGO Project - MS 51-33
Pasadena CA 91125
Phone (818) 395-2129
Fax (818) 304-9834
E-mail: info@ligo.caltech.edu

Massachusetts Institute of Technology
LIGO Project - MS 20B-145
Cambridge, MA 01239
Phone (617) 253-4824
Fax (617) 253-7014
E-mail: info@ligo.mit.edu

WWW: http://www.ligo.caltech.edu/

Characterization of the temporal filtering of an empty BSC of magnetic fields

S. Lefranc

Abstract

At the present time, the LIGO gravitational wave detector is in a final phase of construction. After explaining what is a gravitational wave and theirs possible sources, I will present the LIGO detector and its limitation. Many noise source have been identified, and, due to the choice of permanent magnets to control test mass motion with sufficient bandwidth and strenght, it appears that the magnetic field fluctuations due to internal (electronic systems) and external (thunderstroms) origin could be a possible source of noise, and so, generate pertubations. In order to verify this, I have made measurements inside the BSC of a time varying magnetic field, generated outside, in order to find the time-domain filtering of the BSC and to evaluate the field gradient due to the BSC.

Keywords: LIGO interferometric detector, magnetic noise.

Contents

I would like to really thank all the LIGO group at MIT for its kindness during my stay and the help provided when needed. I especially thank my adviser, David H. Shoemaker and Pr. Rainer Weiss for inviting me to spent this two months of research. I also want to thank Shourov Chatterji to the help he provided.

1. Introduction

Maybe in a near future some humans will visit other stars, and why not other, galaxies using today Science-Fiction technologies. But meanwhile the day a such travel will be possible, we must comtemplate the stars from very far away and search by any ways to pick-up the signal they send. The elderly had theirs eyes to observe and made very slow conceptual or technical progress (with respect to the progress made in the 20th century). Theirs theory tried to explain what they saw. Now there is a lot of theory and the search of a signal as little as it can be, confirm, modify or force them to disappear.

The theory of General Relativity is widely celebrated and often verified with success. The main idea of Einstein was to show that the laws of Physics were the same everywhere. The gravitational wave idea come from this new conception of the Law of Nature. At the present time the only messenger of the information of the universe is the photons, particles associated with the electromagnetic wave. Another particle could be a good messenger, the graviton, associated with the gravitational wave. It is the purpose of LIGO to detect, not the gravitons, but the effect of the gravitational waves on free masses

The Laser Interferometer Gravitational wave Observatory (LIGO) will be operating soon. Due to the tiny variation of distance it must detect, this detector is sensitive to a lot of “noise”. To control the displacement of test masses an electromagnet actuator was choosen which consists of permanent magnets attached to the test mass interacted with fixed coils which carry control current. This choice could lead us to a new kind of “noise”, the one due to the magnetic field caused by an external origin (thunderstrom for exemple). So my task here was to characterize the response of the BSC (Basic Symmetric Chamber) to a time varying field generated outside and determine the magnetic field gradient due to the BSC. It is interesting to present some theory about gravitational waves and theirs sources, as well as LIGO detectors and its noise limitation.

Before begining the measurements, some preparation had to be completed. First I made a magnetic map of the DC field around the BSC. There have been done some modifications in the building to allow the construction of this intereferometer, and there was a high magnetic area before, so the floor was magnetized. After having a better idea of the repartition of the magnetic field around the BSC, I had learned how use a Dynamic Signal Analyzer and established an experimental protocol in order to figure out the best way to generate a field outside the tank that will be strong enough to be measured inside. Some experiments were made in order to have a good idea of what was measured, and it lead me to some modifications in my initial protocol. After modifying my devices to allow them to work in a class room of class 100, I have made the measurements. At last I interpret them in order to find the magnetic field gradient due to the BSC.

2. Theoretical aspect of Gravitational Waves

2.1 Introduction

As the same way as Special Relativity asked for a formulation of the Laws of Nature independent of the Galileo frame and a constant speed-light, the General Relativity is based on two principles: the independance of the Laws of Nature with respect to any frames, and the equivalence between inertial and gravitational masses.

Just as Special Relativity liberated from the notion of ether, General Relativity liberates from the gravitational force, stating the equivalence between inertial and gravitational masses. And the easiest way to consider this equivalence is to assume that the gravitational field curves space. Thus a test mass submissive to it is a mass in free fall along a geodesic of the curve space. Introducing this new notion, Einstein introduced at the same time the notion of gravitational wave, because, as each mass distorting space, if this mass is accelerated, it will creates ripples which propagate.

Then, as any mass curves space-time, we can assume that if this mass oscillates, for example at the end of a spring, it will distort space-time periodically, and this deformations will propagate as a wave on a string. These ripples will be attenuating during theirs displacement like ripples on a lake.

2.2 Gravitational Waves

2.2.1 Weak field approximation

One of the main problem about gravitational waves in particular, and the General Relativity in general is the nonlinearity of Einstein's equations, e.g. the impossibility to exactly solve them in almost every case. As each parts of the universe possess a non-null energy density, it will create a gravitational field, which modify, so a curvature of space-time. But this field contains energy that is also a source of gravity. Likewise the gravitational waves carry energy and then creates itself a gravitational field, which modify the gravitational wave. There is self-interaction and the phenomenon is nonlinear.

One way to solve this problem is to be very far away from the source and consider that the pertubation of the metric due to the gravitational wave is enough small that the problem could be linearised. In this weak field limit, the metric could be approximated as

$$g_{\mu\nu} \approx \eta_{\mu\nu} + h_{\mu\nu}, \quad |h_{\mu\nu}| \ll 1 \qquad \text{(eq. 1)}$$

where $\eta_{\mu\nu}$ is the Minkowski metric. The weak-field Einstein equations in vaccum then take the form (with a suitable choice of gauge)

$$\left(\frac{-1}{c^2}\frac{\partial^2}{\partial t^2} + \nabla^2\right) h_{\mu\nu} = 0 \qquad \text{(eq. 2)}$$

This is clearly a wave equation and the solution can be written in terms of a traveling plane wave:

$$h_{\mu\nu} = h_0 \varepsilon_{\mu\nu} e^{ik_\mu x^\mu} \qquad \text{(eq. 3)}$$

provided k_μ that satisfies $k_\mu k^\mu = 0$. With a further choice of gauge known as the transverse-traceless gauge, the compoments of the (polarization) tensor are much constrained. For a frame in which the wave is traveling in the *z* direction, the origin of the adjectives "transverse-traceless" becomes clear, as the tensor takes the form:

$$\varepsilon_{\mu\nu} = \begin{bmatrix} 0 & 0 & 0 & 0 \\ 0 & \varepsilon_{xx} & \varepsilon_{xy} & 0 \\ 0 & \varepsilon_{xy} & -\varepsilon_{xx} & 0 \\ 0 & 0 & 0 & 0 \end{bmatrix} \qquad \text{(eq. 4)}$$

The above solution describes a quadrupole wave and has a particular simple physical interpretation (see fig. 1): Let's assume two free masses are placed at position x_1 and x_2 *(y=0)* and a gravitational wave with + polarization is propagating along the *z*-axis, then the free masses will stay fixed at their coordinate positions, but the space in between, and therefore the distance between x_1 and x_2, will expand and shrink at the frequency of the gravitational wave. Similarly, long the *y*-axis the separation of two points will decrease and increase with opposite sign. The strenght of a gravitational wave is then best expressed as a dimension-less quantity, the strain *h* which measure the relative lenght change $\Delta L / L$.

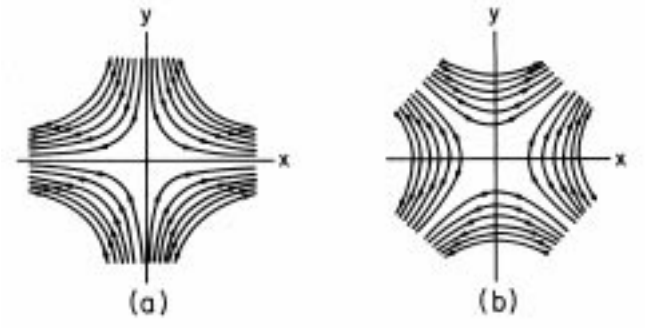

Figure 1: Direction of space deformation for a gravitational wave propagating along the *z*-axis, + polarization (a) and x polarization (b).

Electro-magnetic waves which rea visible to an observer on Earth are usually produced in the outer layers of an astrophysical object, whereas gravitational waves carry information about the inside behaviour and the mass distribution of an object. Arguably, the information obtained by the two will be quite different, and it is difficult to predict gravitational sources from electro-magnetic observations.

2.2.2 Gravitational wave amplitudes

Before looking at possible detection techniques we roughly estimate how large the observed effect of a gravitational wave from an astrophysical source could be. If we denote the quadrupole of the mass distribution of a source by *Q*, a dimensional argument, together with the assumption that gravitational radiation couples to the quadrupole moment only, yields:

$$h \sim \frac{G\ddot{Q}}{c^4 r} \sim \frac{G(E_{asymkin}/c^2)}{c^2 r} \qquad \text{(eq. 5)}$$

with *G* the gravitational constant and $E_{asymkin}$ the non-symmetric part of the kinetic energy. If ones sets the non-symmetric kinetic energy equal to one solar mass,

$$E_{asymkin}/c^2 \sim M_{sun} \qquad \text{(eq. 6)}$$

and if one assumes the source is located at inter-galactic or cosmological distance, respectively, one obtains a strain estimate of order:

$$h \approx 10^{-21} \quad \text{Virgo cluster} \qquad \text{(eq. 7)}$$

$$h \approx 10^{-23} \quad \text{Hubble distance} \qquad \text{(eq. 8)}$$

By using a detector with a baseline of 10^4 m the relative lenght changes become of order:

$$\Delta L = hL \leq 10^{-19}\,\text{m to } 10^{-17}\,\text{m} \qquad \text{(eq, 9)}$$

this a rather optimistic estimate. Most source will radiate significantly less energy in gravitational waves. We add that the observable effect is not small because the radiated energy is small, in contrary it is huge, but rather becausespace-time is a stiff medium.

2.2.3 Gravitational wave frequencies

Similarly one can estimate the upper bound for the frequencies of gravitational waves. A gravitational wave source can not be much smaller than its Schwarzwild radius $2GM/c^2$ and can not emit strongly at periods shorter than the light travel time $4\pi GM/c^3$ around its circumference. This yields a maximum frequency of

$$f \leq \frac{c^3}{4\pi GM} \sim 10^4 \,\mathrm{Hz} \;\; \frac{M_{sun}}{M} \qquad \text{(eq. 10)}$$

From the above equation one can see that the expected frequencies of emitted gravitational waves is the highest for massive compact objects, such as neutron stars or solar mass black holes.

2.2.4 Experimental evidence for gravitational waves

The only experimental evidence for gravitational waves comes from the timing of binary pulsars systems. these systems consists of two neutron stars orbiting each other. To be observable one of them must be active and emit radiowaves. Since pulsars emit radiowaves mainly along their magnetic axis and since their rotating axis does not have to be aligned with the magnetic axis, Earth-based radio antennae can observe a periodic radio signal if the system is aligned so that the radio beacon passes ove the Earth. the frequency of this signal is determined by the rotation period of the pulsar and is typically of vey high precision.

In a double neutron star system this periodic signal is modulated by the orbital frequency of the two neutron stars and can therefore be used to precisely deterine the orbital period and phase. The first double pulsar system, PSR B1913+16, was discovered by Hulse and Taylor in 1974. Its orbital period is 8 hours. The emission of gravitational waves brings the two neutrons stars closer together, and thus increase the orbital frequency. The loss of potential energy in this system is in agreement with the emission of gravitational waves predicted by General Relativity. As a consequence, the two neutron stars will merge in about 300 million years.

2.3 Astrophysical sources

2.3.1 Coalescing compact binaries

Compact binaries are among the best candidates to be the first seen by an Earth-based gravitational-wave antennae. compact binaries can consist of either two neutron stars, two black holes, or one of each. Due to their small size, they can orbit each other at close range and a high orbital frequency. Being very close and rotating fast means that the second time derivative of the mass quadrupole moment is large and, hence, gravitational waves are emitted with a high efficiency. Indeed, the radiated energy is so large,

that a double neutron star system which is 500 km appart will loose all its potential energy within a couple of minutes.

The waveform is a chirp signal (see fig. 2): increasing both in amplitude and frequency with time, until the two objects are close enough to merge.

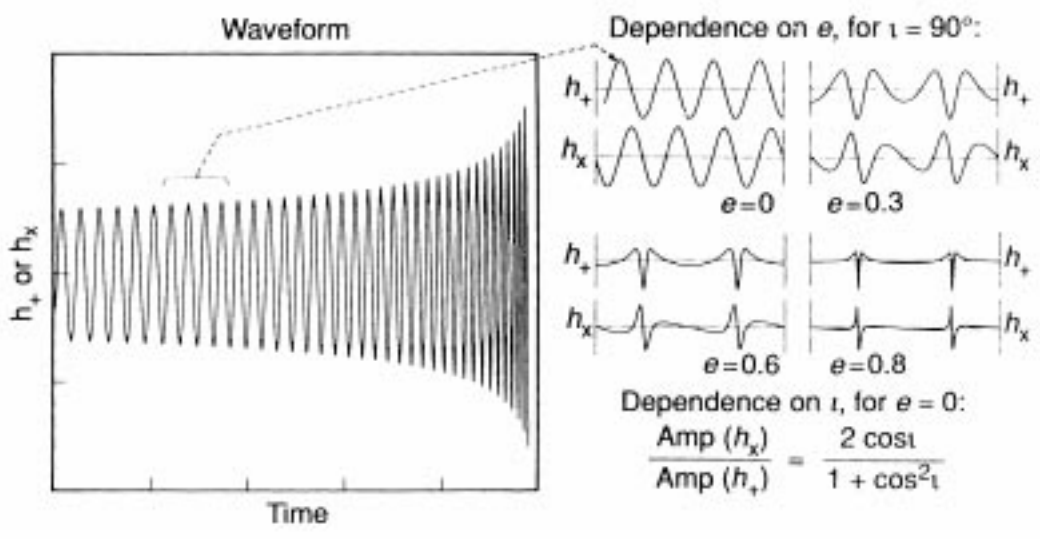

figure 2: Chirp waveform from an inspiral event of a compact binary sytem. On the right hand side the dependency of the waveform on the orbital eccentricity *e* and the orbital inclinaison *i* is demonstrated.

2.3.2 Binary stars

Ordinary binary stars are one of the most reliably understood sources for periodic gravitational waves. Binary stars typically have orbital periods larger than an hour and, correspondingly, gravitational waves frequencies $f \leq 10^{-3}$ Hz. This means that only space-based detectors will be able to detect them by integrating over long time periods.

2.3.3 Rotating neutron stars

A rotating neutron star will emit gravitational waves if its mass distribution is non axis-symmetric along the rotation axis. A non axis-symmetric mass distribution could be due to extremely strong magnetic field which deform the star, due to its past history which created the star in a deformed state, or due to accretion of matter from a companion star.

2.3.4 Supernovae

Supernovae have all the attributes associated with a good gravitational wave source: they weigh several masses, they are compact and they experience large accelerations. However gravitational radiation only couples to a changing quadrupole moment

and, hence, if a supernovae collapse and the subsequent explosion have an axial symmetry, no gravitational waves are emitted. They are several possible mechanisms which could overcome this deficit:

- Initial density and temperature fluctuations may trigger the collapse unevenly.
- High rotation speeds can lead to a bar instability.
- Hydrodynamic instabilities could introduce large convection streams which may effect the initial implosion.
- A reminiscent neutron star may experiencea strong boiling shortly after its formulation.

It is unlikely that each and every supernovae event will be exactly axis symmetric, but how large the asymmetric are and how often these asymmetries lead to detectable gravitational waves is very much uncertain at this time.

2.3.5 Supermassive black holes

An other good sources of gravitational waves are supermassive black holes $(M > 10^5 M_{solar})$ eating surrounding objects. However, due to their size, the frequency band of interest is lower than the one for the above sources. Typical frequencies are in the mHz regime and will not be accessible by Earth-based observations due to limitations posed by seismic activities and gravity gradient noise (see next chapter). Nevertheless, these sources are prime candidates for space-based antennae.

3. Laser interferometers

The idea of detecting gravitational waves using a Michelson interferometer was discoverd by several group independantly, and lead to the first prototype of an interferometric detector. The idea took a significant step forward when Rainer Weiss performed a study which identified all the important noise sources which limit the instrumental sensitivity (see next section).

There is two complementary approaches to detect gravitational waves with laser interfrometer: space-based and Earth-based. A space-based antennae is free from seismic excitations and can utilize long arm lenghts of order 10^{10} m. It is best suited to detect gravitational waves in a frequency band between 10^{-4} Hz and 10^{-1} Hz. An Earth-based antennae is limited by gravity gradient noise below a couple of Hz. In reality, seismic noise probably sets this limit even higher. Earth-based detectors have their best sensitivity in a frequency band between 10^{1} Hz and 10^{3} Hz.

3.1 LIGO detectors

The LIGO project is a collaboration between MIT and Caltech. It is composed of two widely separated interferometer to allow coincidence measurements. The arms of the interferometers are long of 4 km. All Earth-based interferometric gravitational wave detector share a similar design philosophy. The design of these detectors is driven by the goal to minimize the effects of noise on the instrumental sensitivity. All designs use in-vaccum suspended optics builds on top of a seismic isolation system for their main interferometer mirrors. Similarly, all designs use a highly stabilized laser source in conjonction with a mode cleaner to deliver a high quality laser beam to interferometer. They all incorporate an optical configuaration which recquires an active control system for microscopically adjusting cavity and Michelson lengths, in order to counteract drifts and fluctuations introduced by seismic activities.

Figure 3: LIGO interferometer at Hanford site

3.2 Noise sources

Measuring length deviations smaller than the proton radius puts high recquirements on the technology used to build these instruments. It also recquires a good understanding of technical and physical noise sources which possibly limit the gravitaional wave sensitivity. The design sensitivity of the LIGO project is shown in fig. 4. It shows that the sensitivity at low frequency, $f < 50$ Hz, is due to seismic noise, at intermediate frequencies, $50 < f < 150$ Hz, due to thermal noise and at high requencies , $f >$150 Hz, due to laser shot noise. Only noise sources for initial Earth-based interferometer will be explained.

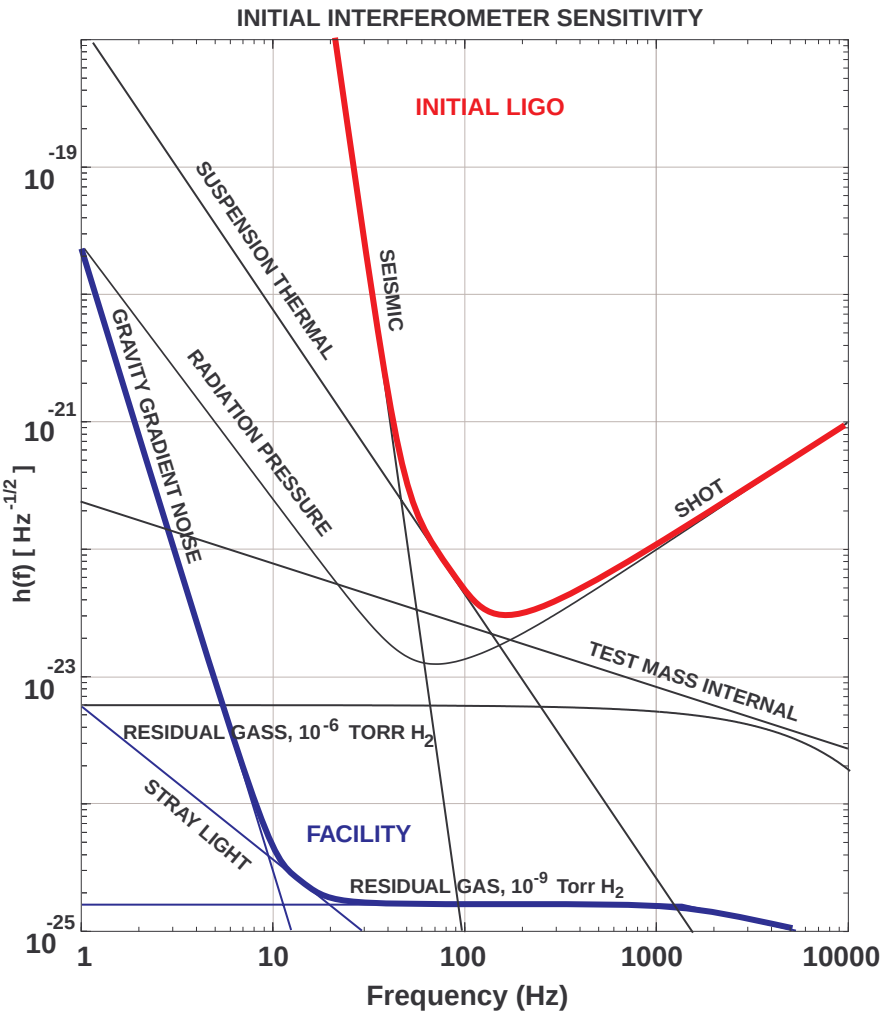

Figure 4: Design sensitivity for LIGO. The plot shows that the initial strain sensitivity is limited by seismic, thermal and shot noise. These are technical noise sources which can be improved on in future designs. The plot shows the gravity gradient, the scattered light and the residual gas noise which ultimately will limit the sensitivity of Earth-based detectors.

3.2.1 Photons shot noise

The fluctuations of the number of photons in the input beam causes fluctuations of the signal at the anti-symmetric port. For a power-recycled Michelson inteferometer with Fabry Perot arm cavities one obtains an equivalent shot noise limited strain sensitivity of:

$$h_{shot}(f) \sim \frac{\sqrt{1+(f/f_{FPI})^2}}{N_{bounce}} \cdot \frac{\lambda}{2\pi L} \cdot \sqrt{\frac{h\nu}{G_{RC}P_{in}}} \qquad \text{(eq. 11)}$$

with f_{FPI} the cavity pole, N_{bounce} the average number of effectives bounces in the arms, λ and ν the laser wavelength and frequency, respectively, L the arm length, the power recycling gain and P_{in} the input laser. Fig. 5 shows the sensitivity spectrum of the phase noise interferometer at MIT, demonstrating that it is technically possible to achieve shot noise limited sensitivity above a couple of 100 Hz.

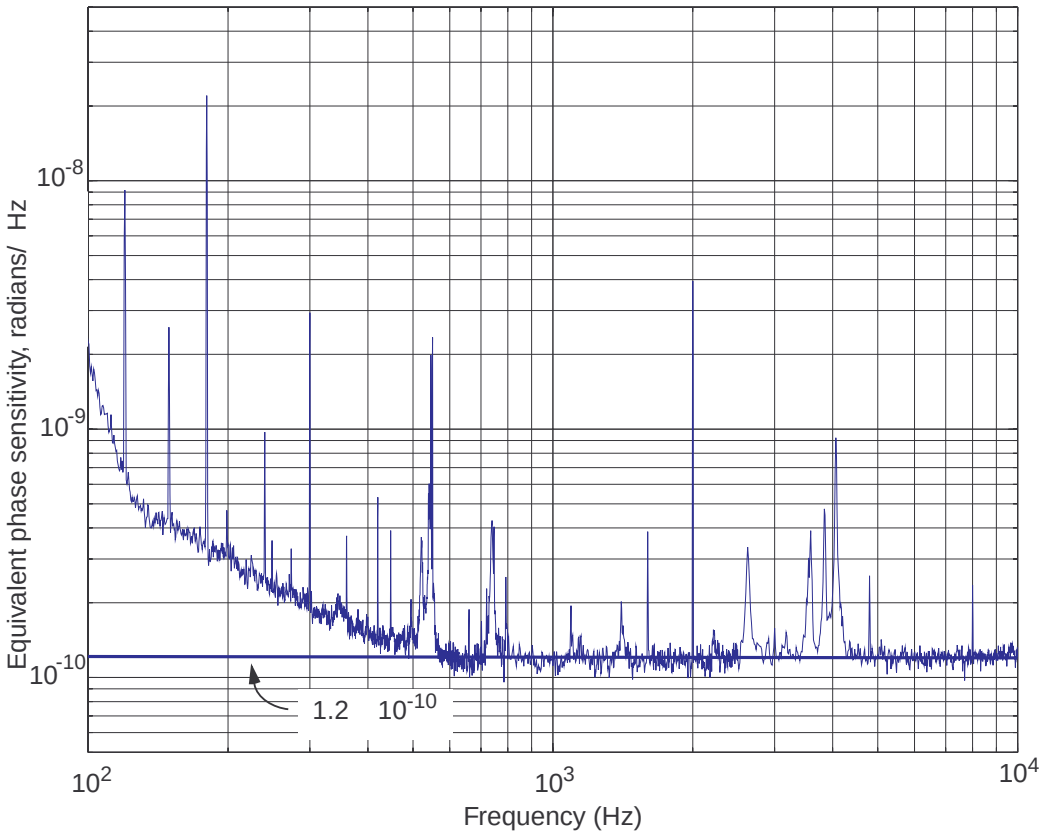

Figure 5: Spectral sensitivity of the MIT phase noise interferometer. Above 500 Hz the spectrum is shot noise limited at the level close to the one needed for initial Earth-based detectors. The additional features seen in the spectrum are due to 60 Hz powerline harmonics, wire resonance (500 Hz-600 Hz), optical mount resonances (700 Hz-800 Hz), calibration line (2 kHz) and resonance of the magnets (4 kHz).

3.2.2 Seismic noise

The Earth surface is in constant motion because of seismic and volcanic activities, because of ocean waves “hammering” on the shores, because of wind and because of the tidal force of the moon. Seismic noise is most pronounced at low frequencies (0.1 Hz to 10 Hz) and falls off quickly at higher frequencies. Typical seismic noise levels are:

$$x(f) \approx 10^{-9}\ \mathrm{m}/\sqrt{Hz} \qquad \text{for} \quad 1\ \mathrm{Hz} < f < 10\ \mathrm{Hz} \qquad \text{(eq. 12)}$$

$$x(f) \approx \frac{10^{-7}}{f^2}\ \mathrm{m}/\sqrt{Hz} \qquad \text{for} \quad f > 10\ \mathrm{Hz} \qquad \text{(eq. 13)}$$

For initial Earth-based interferometers roughly an attenuation of 9 orders of magnitude is recquired at frequencies around 100 Hz.

3.2.3 Thermal noise in the suspension elements

Thermally driven motions of the test masses (optical components) will limit the initial sensitivity of Earth-based detectors in the intermediate frequency range around 100 Hz. The magnitude of these motions depends on $k_B T$. To investigate the effect of thermal noise one has to look as its spectral density. There is a deeper connection between the dissipation mechanism of a system and the power spectral density of the random displacements. Low loss systems typically have high Q resonances. Most of the random motion is concentrated in a small bandwidth around these resonances. By decreasing the dissipation of a system, one can incease the Q and at the same time reduce the spectral density of the random dispalcements away from resonance.

A simple way to obtain a low loss system is to suspend the test masses in a form of a pendulum. The restoring force of a pendulum has two components: gravity and elasticity of the suspension wire. For all practical purposes the “gravitational spring” is lossless, and only the elastic constant has a dissipative fraction. As long as the wire is reasonably fine, the elastic spring constant is much smaller than the gravitational spring constant. Typically, the pendulum frequency for a suspended test mass is around 1 Hz. Above resonance the spectral density falls as $f^{5/2}$ (frictional damping).

The effect of the thermal noise on the strain sensitivity of an interferometer is proportionnal to the average number of effective bounces of the laser beam. This is the main reason to favor a long baseline design with a low number of bounces over a shorter design with a higher number of bounces.

The sensitivity of the curve of the Caltech 40 m is shown in fig. 6. It clearly demonstrates the importance of thermal noise.

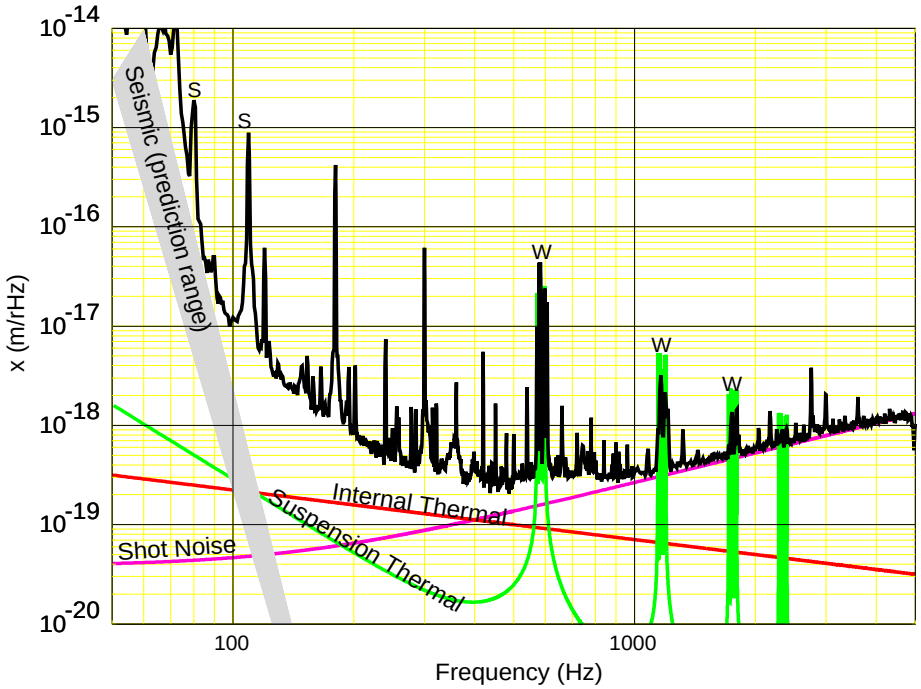

Figure 6: spectral sensitivity of the Caltech 40 m interferometer

3.2.4 Thermal noise driving mirror normal modes

The equipartition theorem states that energy eigenmode of a system is excited by thermal noise to a mean energy $k_B T/2$. This is also true for the "drum" modes of the test masses. Typically, the frequencies of these eigenmodes is in the kHz regime.

4. Experiments

4.1 Devices used

To Complete the measurements I have used different devices. For reference, I explain briefly how they work. I especially dwell on the way chosen to generate a time varying field.

4.1.1 Magnetometer

It is a Bartington MAG-03MCES100, a compact triaxial flux-gate sensor which requires a power supply of between $\pm 10\,\mathrm{V}$ and $\pm 17\,\mathrm{V}$ and provide three analog outputs of $\pm 10\,\mathrm{V}$ full scale, proportional to the magnetic field along each axis. For a unit with a full scale range of $\pm 100 \mu T$ the output voltage for each axis is $0.1 V/\mu T$ of field in the direction of that axis. The frequency response is maximally flat from DC to at least 1 kHz.

4.1.2 Power Supply

It is a MAG-03PSU which is specially designed for the magnetometer. The input is connected to the magnetometer, and there is three outputs that corresponds to the x,y,z components of the field.

4.1.3 Dynamic Signal Analyzer

The Dynamic Signal Analyser (DSA) is a very usefull and complex device which allows transfer functions to be measured (among other things). Basically, the DSA is composed of several input channels, and a source. We use the source to drive a device as we use as input, and we take the response of the device as an output. We only use the DSA with a swept sine mode: the analyser outputs a sine wave which is stepped accros the frequency span. We can set the number of steps, or measured points, by specifying the sweep resolution.

4.1.4 Excitation coil

As we want to know the time-domain filtering of the BSC to a field, it was necessary to generate a time varying field. A magnetic field is a function of the shape of the source which generates it (following Ampere's law). The idea was to use a big circular coil with a diameter of 1.5 meters, and for this kind of coil, we can easily show using the Biot and Savart law that the field generated along its axis is:

$$B_z(f) = \frac{\mu_0 N I R^2}{2(R^2 + z^2)^{3/2}} \qquad \text{(eq. 14)}$$

where:
I is the current that pass through the coil,
R is the radius of the coil, e.g. 1.5 meters,
z is the vertical coordinate along the axis,
N is the number of turn in the coil, e.g. 216 turns.

Then, for a fixed vertical coordinate, the only way to make a time-dependant field is to change the value of the current. But we are only able to modify the voltage that we send into the coil. Fortunately, we can model the coil by a RL circuits. In this case, the current can be written as:

$$|I| = \frac{|V|}{\sqrt{R_{es}^2 + L^2 \omega^2}} \qquad \text{(eq. 15)}$$

where:

$|V|$ is the voltage in the coil,
L is the inductance of the coil, e.g. $0.19H$,
R_{es} is the resistance of the coil, e.g. 42.5Ω.

So, if we want to change the current in the coil, as the resistance and the inductance are constant, we just have to change the voltage that we send in this coil. The B-field generated by the coil is function of the frequency, we can rewritte (eq. 14) as:

$$B_z(f) = \frac{\mu_0 N R^2}{2(R^2+z^2)^{3/2}}\left(\frac{|V|}{\sqrt{R_{es}^2 + L^2 4\pi^2 f^2}}\right)$$

We are going to use the swept mode of the Signal Analyzer to generate this voltage in the coil.

4.2 Map of the DC field around the BSC

4.2.1 Measurements

The mapping of the DC field was quite important because of the experimental protocol I have designed. As the coil that generates the field was on the floor, it was important that the magnetometer we used as a reference was not saturated by a parasitic field and enable us to do correct measurements.

As we are only interested in the DC components of the field (this is the same as measuring the Earth magnetic field, if there is no “magnetic pollution”) we directly connect the output of the magnetometer to a voltmeter. With the specifications provided in part 4.1 we see that when we measure something in Volt in the voltmeter, we have to multiply it by 10^{-5} to have a field in Tesla.

After made the measurements, I have used the software MATLAB in order to have a plot of the intensity of the magnetic field. The program is available in the appendix (7.1).

4.2.2 Results

Using the program and the data I acquired, we are able to plot the magnitude of the B-field with respect to the position on the grid. The color is used to express the intensity of the field. Blue is for the lower intensity and red is for the higher ones. The three different axis are labelled with SI units. the points represent the place where the measurements were done.

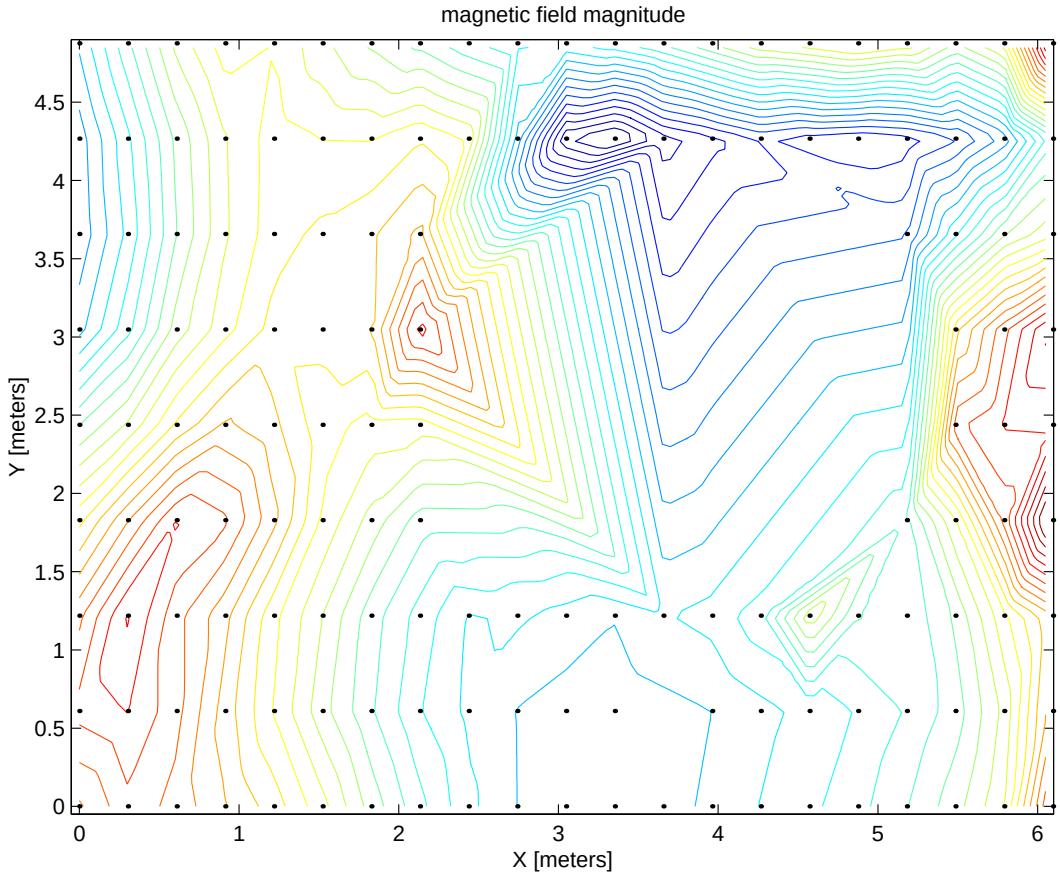

Figure 7: Contour of the intensity of the B-field around the BSC.

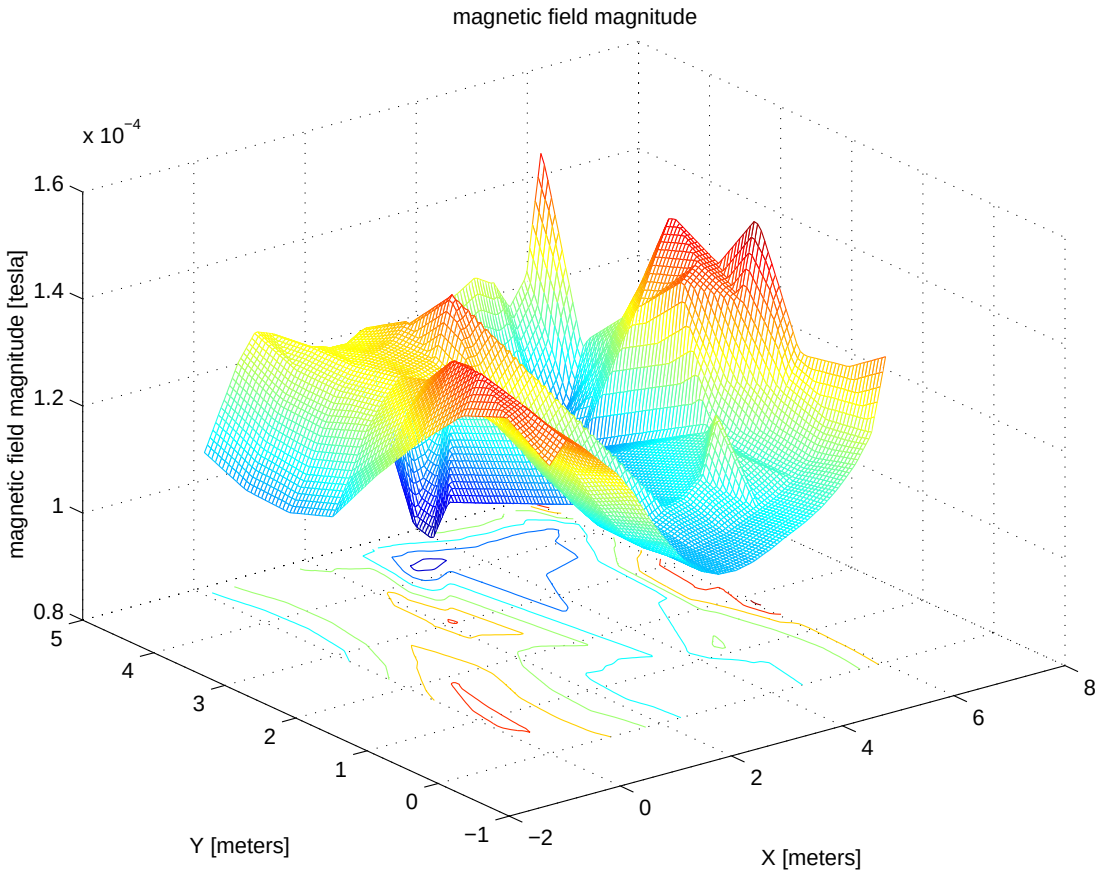

Figure 8: 3D representation of the variation of the B-field around the BSC.

From these two plots we can see an area of low magnetic field intensity centered around the location of the BSC and two areas of high magnetic field intensity which are on both side of the area of low field intensity.

We see on the figure 8 that the amplitude of the field around the BSC varies between 0.08 and 0.16 mT; if we consider that the average intensity of the Earth magnetic field is 0.05 mT that leads us to the conclusion that the floor of highbay is slightly magnetized, but probably not enough to modify the measurements. Nevertheless, we must be very careful with this conclusion:

- First, the magnetometer was not put at the level of the ground, but at approximately 90 centimeters, so if there is an important magnetic field on the floor, it is possible to not have measured it.

- Second, our measurements are, at maximum, three times higher that the Earth magnetic field. It is not a big difference, and it could be due to some variation of this field, which is not constant on Earth.

Unfortunately it seems that the floor was, at some point, magnetized because some other measurements made when we were using the coil show us that the magnetometer was saturated. I also realized that some of the measurements I made saturated the magnetometer. As its ouput range is 10 Volts, a DC field of 10^{-4} Tesla suffices to saturate it. We see on the figure 8 that we are at the limit of saturation. We have to conclude that the floor of the highbay is magnetized, and a further analyze of it with more sensitive magnetometer should be do.

In order to avoid pertubation of the DC field during my measurements, at the place where the coil was put, I made measurements of the DC field and they were similar to the Earth magnetic field. We were lucky because, as we are going to see in the next section, the protocol established needs a magnetometer in the center of the coil to be used as a reference, and it will be very tedious to not measure exactly the field generated by the coil.

4.3 Measurements inside the BSC

4.3.1 Experimental protocol

The idea to make measurements inside the BSC was simple: Generate a time-varying field outside the tank and measure it inside. But we preferred not to open the BSC. Thus, first we must open one of the several ports of the tank, and second we must work in a clean room area.

In the picture of the BSC with the clean room (see appendix, 7.4) one sees several ports at different heights. There were two reasons that lead me to the choice I made for the ports I opened: First, I am interested to know the magnetic field around the position of the test mass and second, a quick calculation show me that if I open the big port (which is a very heavy operation, it weights half a ton), it will significantely modify the magnetic field inside the tank. These two reasons lead me to the conclusion that it is enough to open a little port which is at apporximately the same level as the test mass is.

Fortunately, the clean room that already exists was high enough to access these ports. I made an extension on this clean room to allow it to access on a side of the BSC. To verify the cleanliness of the clean room, I used a counter of dust particles. My goal was to work under a clean room of class 100 (it signifies that the counter of particles counts 10 particles during 1 minute). When I made the measurements I checked often with the counter, and all of them were made between class 60 and 100. The class was slighty higher in the table on which I worked, but near the ports it was always around 60-80. I consider that the measurements were made under a good clean room protocol.

4.3.2 Measurements

During the experiments, the problem was to be sure to exactly measure what we wanted. In order to verify this, I made the following experiments:

• The signal analyzer sends a voltage into the coil. We use the signal of a magnetometer in the center of the coil as output, and the input is the source voltage send by the DSA. We can model this by:

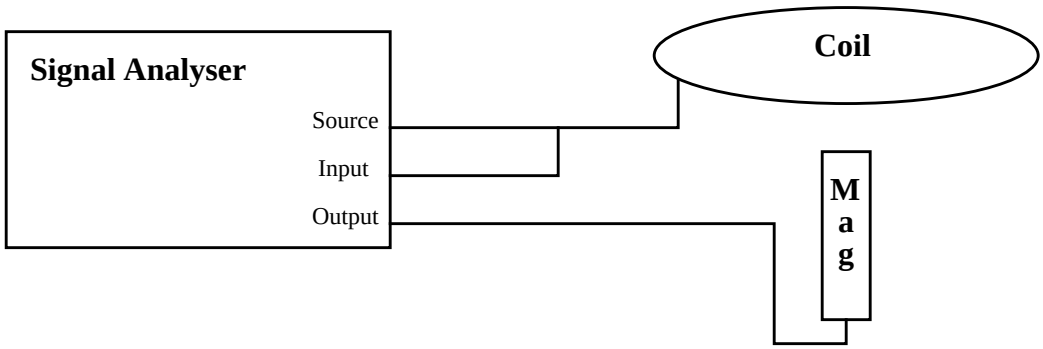

The result of this experience is predictable: In theory, the quantity measured by the magnetometer should be the same as the one send into it, so if we make a transfer function plot of the Ouput/Input it should be a line. It was made and the result was not a as desired.

We can explain this by the effect of the inductance in the coil. When the frequency increasases, the effect of the inductance increases too, it is very evident on (eq.15). To avoid this, it was decided to put a second magnetometer in the center of the coil as input. We can model this by:

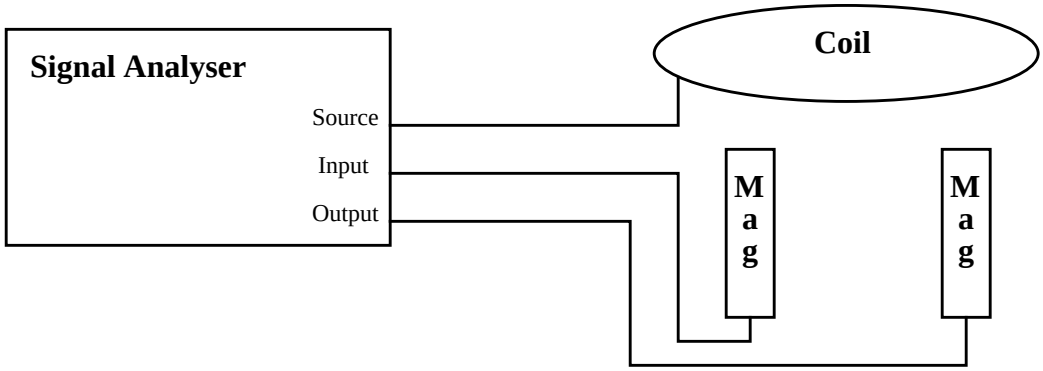

If we do a transfer function measurement of this new configuaration with the 2 magnetometers in the center of the coil, as they exactly measure the same thing, we obtain a line.

• Another problem was to be sure that the magnetometer inside the tank will receive a signal, e.g., that the B-field generated by the coil was enough intense. There is no very good way to assure this. One could be the generation of a very strong B-field, but it was not possible with the devices I used, so I decided to do the following experiment:
I put the magnetometer inside a metal box and acquired a set of data. They show that the B-field was enough important to be detected by the magnetometer. And even if the shield

effect is not so important as the one produce by the tank, I consider that is an enough good result to hope detect a signal inside the BSC.

- The last problem, but not the least was to find a system to handle the magnetometer and allow us to measure in many dimensions. I have made a kind of boom with which we can measure in two dimensions:

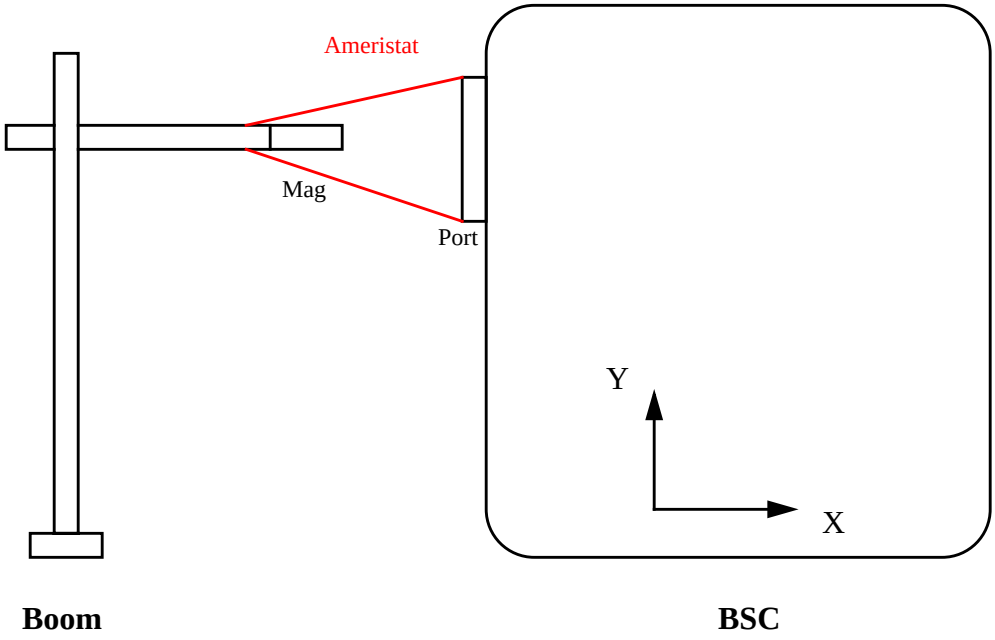

Figure 9: Description of the methods used to acquire data inside the BSC.

With this system it was possible to make measurements at three differents heights: 177.5 cm, 179.5 cm and 181.5 cm. I was not limited on the X axis, and I decided to make a set of measurements at 30 cm, 60 cm, 80 cm and 100 cm from the edge of the BSC. The center of the BSC is at 130 cm away from the edge of the tank, but I was not able to do measurements at this location, due to the limitations of my devices. I estimate the imprecisions of the boom at 5 cm.

- To satisfy the clean room conditions, the boom was made of plasitc without magnetic properties, and everything was packed with Ameristat (a very clean plastic). To avoid that a big open surface is let in contact with the ambient air, I made a sort of tube with Ameristat, that linked the port of the BSC to the probe of the boom. It is represented in red on the previous picture. With this protection the inside of the tank was not in contact with the ambient air during a very short time.

- The bandwidth of the swept sine is from 1 Hz to at most 1.2 kHz because the magnetometer is not enough sensitive for higher frequencies. The voltage received by the coil is 5 Volts.

4.3.3 Results

I have made ten measurements inside the clean room (X represents the distance in centimeters from the edge of the BSC, and Y is the high on centimeters from the floor).

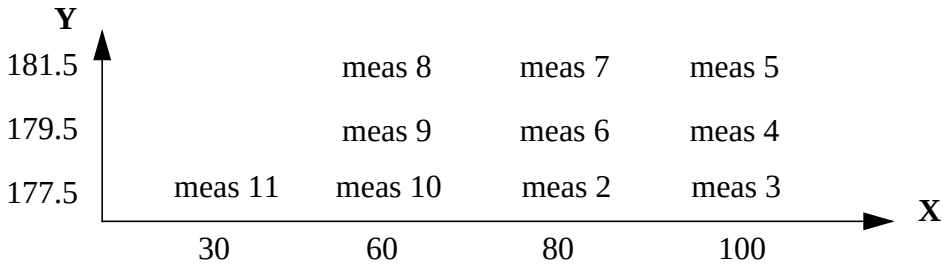

We obtain the following plots (some of them are not represented because the informations they provide are not significant, due to the fact that the different heights are very close: 0.02 meters). I keep the class of plot at Y=177.5 cm because it is very close to the height of the test mass.

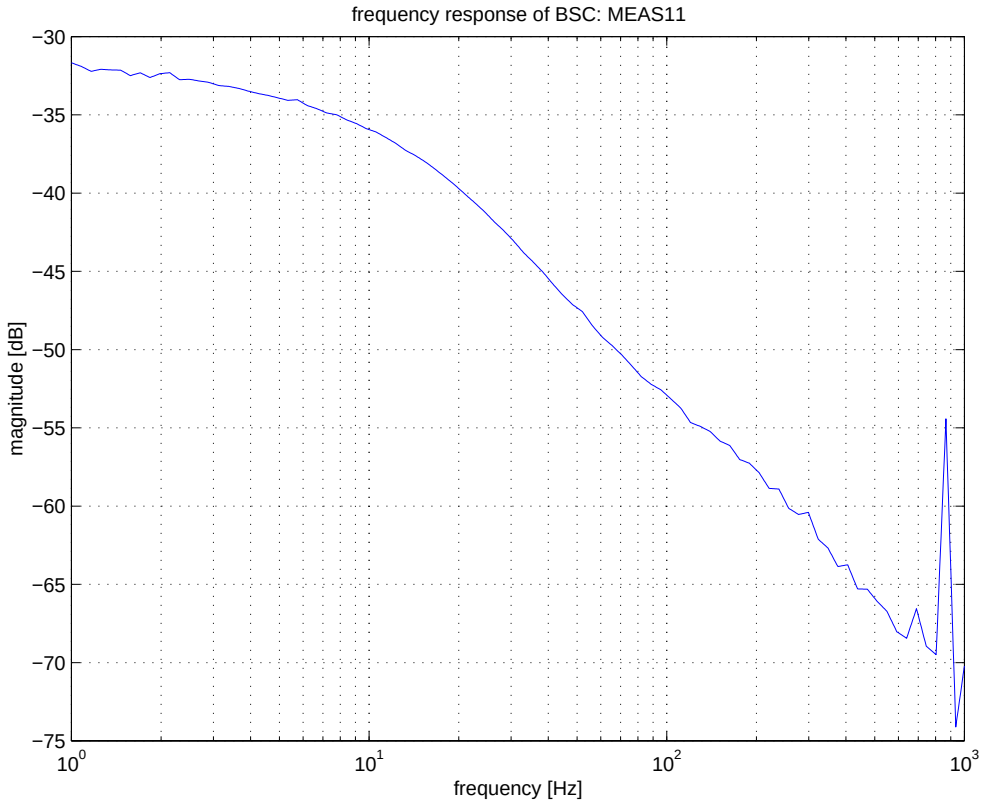

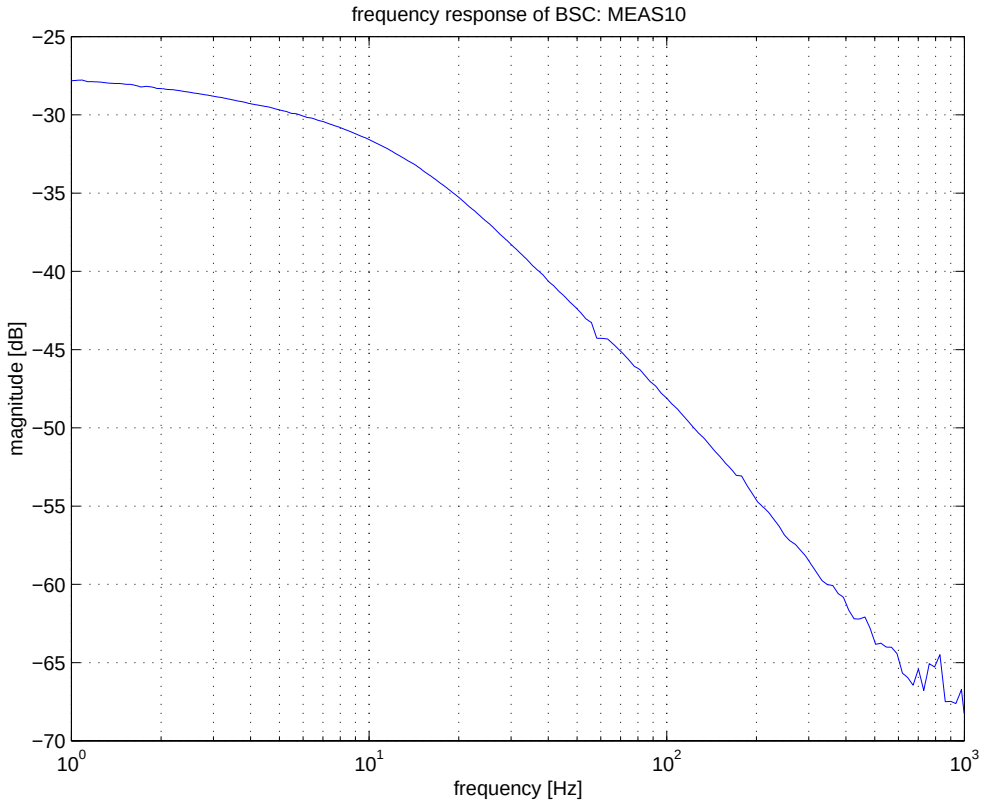
frequency response of BSC: MEAS10
magnitude [dB]
frequency [Hz]
−25
−30
−35
−40
−45
−50
−55
−60
−65
−70
10^0
10^1
10^2
10^3

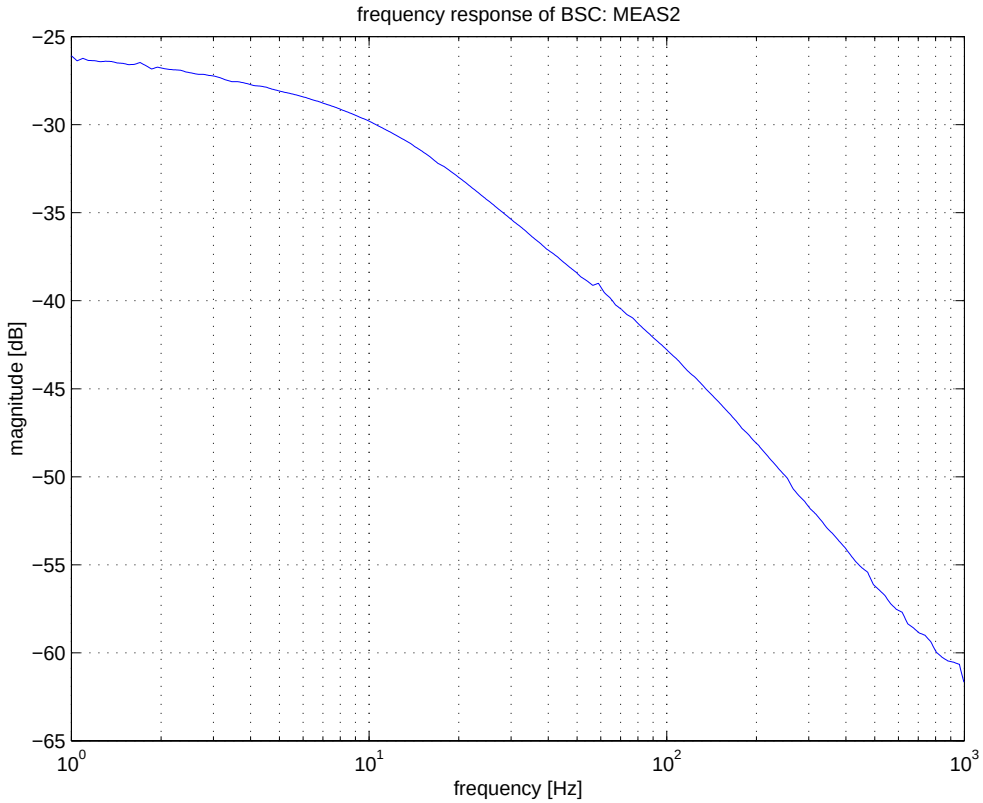
frequency response of BSC: MEAS2
magnitude [dB]
frequency [Hz]
−25
−30
−35
−40
−45
−50
−55
−60
−65
10^0
10^1
10^2
10^3

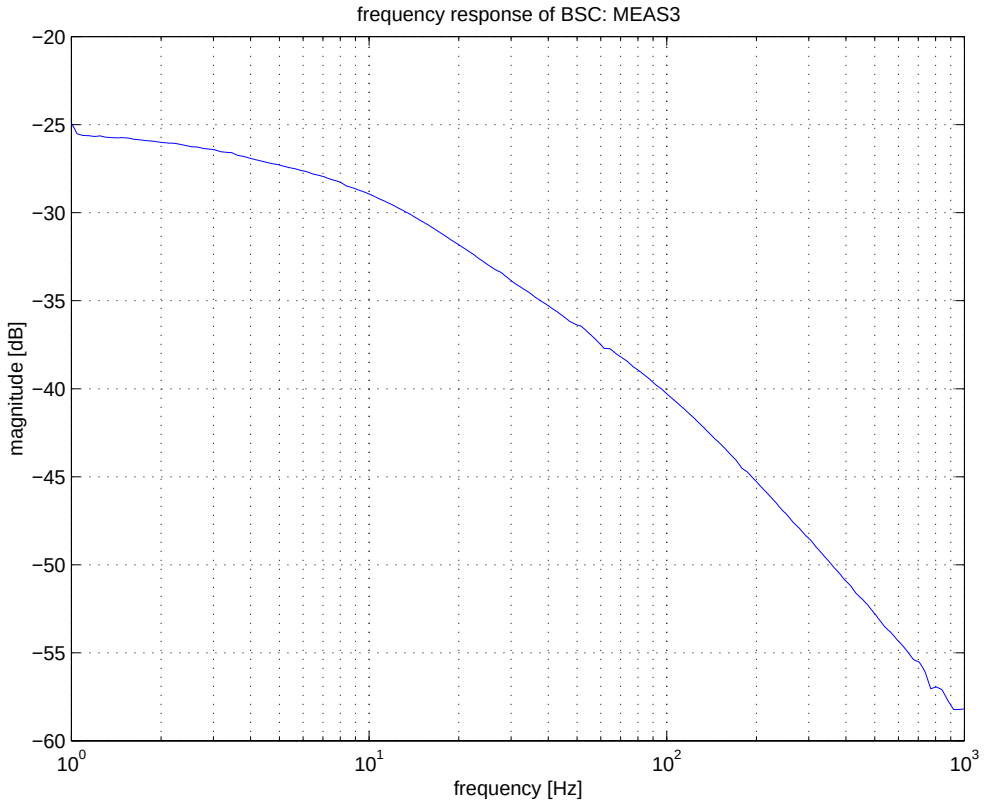

All these plots have the same shape, the one of a low pass filter with a cut-off frequency at 9 Hz (measured with the signal analyzer). The only difference is on the amplitude of the plot. It decreases when we are closer from the edge of the BSC. It is due to the fact that the generated magnetic field is more intense along the axis of the coil, and when we move the magnetometer from this axis, it detects a lower magnetic field. Another reason is the presence of a field gradient that is created by the BSC. This second reasons will be discussed in part 5.2.

A good explanation of the physical meaning of this cut-off frequency was found in [1]. The purpose of this calculation is to show that with very rough approximation about the BSC (cylinder of uniform thickness and conductivity), we can find a cut frequency at the same order as the one we measured, and explain that this frequency is due to a shield effect produce by the BSC.

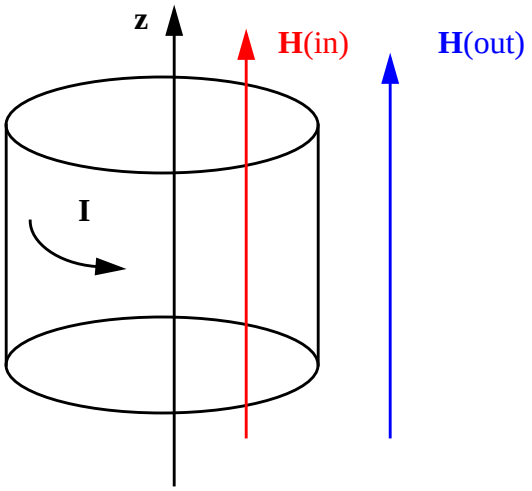

I: surface current density

H(out): magnetic field outside the cylinder

H(in): magnetic field inside the cylinder

The current density J is a divergence free. If we picture the current density flowing in a planes perpendicular to the z axis, and as essentially uniform over the thickness δ of the cylinder, then the surface current density must be independant of the azimuthal position in the cylinder.

$$I = I(t)$$

Ampere's continuity condition, requires that the adjacent axial fields be related to this surface current density by:

$$J = -H_{out} + H_{in} \qquad \text{(eq. 16)}$$

In general, J is not known. To relate it to the axial field, we must introduce the law of Ohm and Faraday. As J is uniform, it is possible to exploit the integral form of the latter law, applied to a contour C that circulates through the cylinder.

$$-\oint_C (E \cdot ds) = \frac{d}{dt}\int_S (B \cdot da) \qquad \text{(eq. 17)}$$

To replace E in this expression, we multiply $J = \sigma E$ by the thickness δ to relate the surface current density to E, the magnitude of E inside the cylinder.

$$I \equiv \delta J = \delta\sigma E \Rightarrow E = \frac{I}{\delta\sigma} \qquad \text{(eq. 18)}$$

If δ and σ are uniform, then E (like I) is the same everywhere along the cylinder. However, either the thickness or the conductivity could be functions of azimuthal position. If σ and δ are given, the integral on the left in (eq. 17) can be taken, since I is constant. With s denoting the distance along the contour C (eq. 17) and (eq. 18) become:

$$-I\oint_C \frac{ds}{\delta(s)\sigma(s)} = \frac{d}{dt}\int_S (B \cdot da) \qquad \text{(eq. 19)}$$

We consider that for the BSC the thickness and conductivity are uniform, so (eq. 19) becomes:

$$\frac{IL}{\delta\sigma} = \frac{d}{dt}\int_S (B \cdot da) \qquad \text{(eq. 20)}$$

with L denoting the peripheral lenght of the cylinder. Representing Ohm's law and Faraday's law of induction, (eq. 20) becomes:

$$-\frac{I}{\delta\sigma}2\pi r = \frac{d}{dt}(\mu_0 \pi r^2 H_{in})$$

With (eq. 16) that represents Ampere's law, H_{out} is a given driving field, so they can be combined into a single differential equation for either J or H_{in}, Choosing the latter, we obtain:

$$\frac{dH_{in}}{dt} + \frac{H_{in}}{\tau_m} = \frac{H_{out}}{\tau_m}$$

where

$$\tau_m = \frac{1}{2}\mu_0 \delta\sigma r$$

is called the *magnetic diffusion time*. With the dimensions of the BSC, we obtain a theoretical magnetic diffusion time of 1/3 s. If we convert that into a frequency, we obtain the cut frequency of the response of the BSC to a magnetic field of 3 Hz, which is the same order as the value measured inside the BSC (9Hz).

A perfect conductor would shield out the magnetic field forever. A physical conductor shield it out for times $t \ll \tau_m$. It signifies that after a time τ_m the BSC does not shield out an exterior magnetic field. We can represent what happened with a drawing (the red lines represeth the magnetic field):

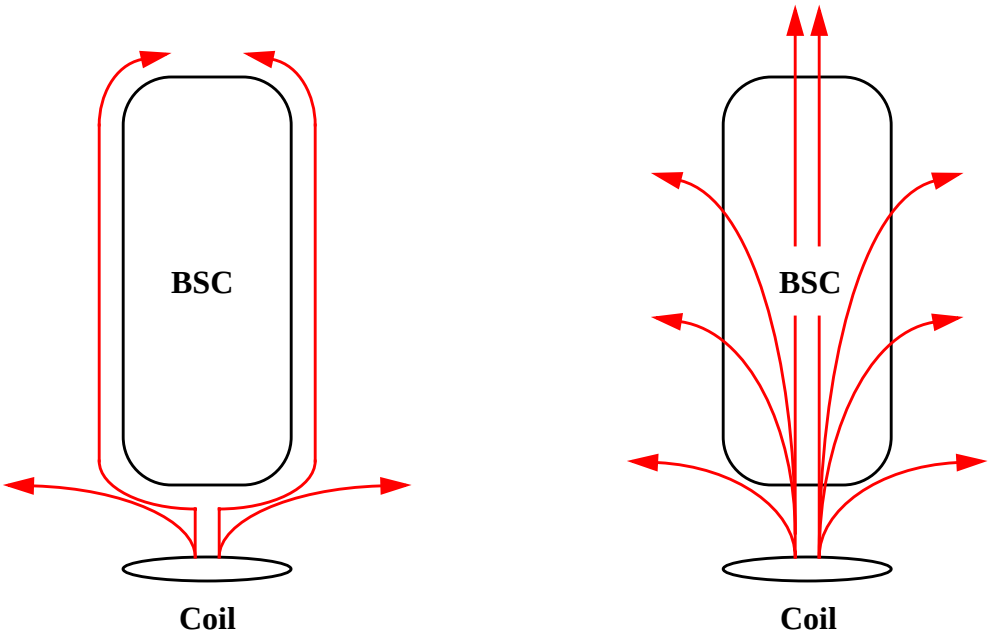

at $t = 0$ seconds at $t \gg \tau_m$

Figure 10: Evolution of the lines of magnetic field with respect to the time

But, if the shape of the plot was only due to this cut frequency, when we superpose them, they should de identique. Or in reality there is a slighty difference between them which is due to the magnetic gradient induces by the BSC. This very important for LIGO and we will see why in the next parts.

5. Implications for LIGO

5.1 Magnetic actuators design

In order to control test mass motion with sufficient bandwidth and strength, a system of an electromagnetic actuator was chosen. It consists of permagnents magnets attached to the test mass interacted with fixed coils which carry control current. You can have a good idea of this on the following picture (fig. 11).

Six magnet assemblies are attached to the optical compoment: four on the front surface- and two on the side surface of the optical compoment. The magnets are placed so that polarities of the magnets alternate, this is to reduce the interaction with external magnetic fields.

With this configuaration, the dipole moment vanishes, leaving aquadrupole moment. In order to know if a magnetic field could have an effect on the optics, it is important to know:

- The magnetic gradient, only due to the tank, around the position of the optics.

- What kind of gradient could pertubates the quadrupole moment and cause significant modifications in the position of the miror that the servo-contro system could not correct.

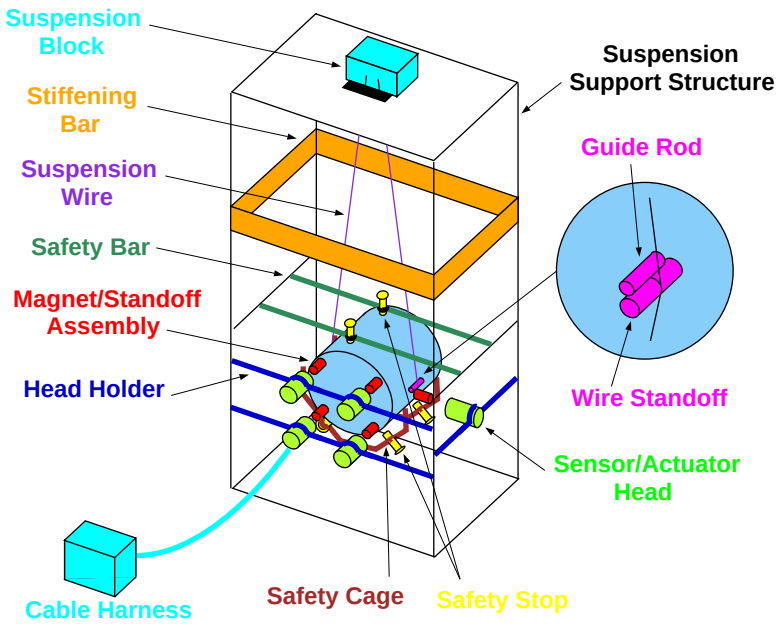

Figure 11: Design of the test mass's support system and actuators

5.2 Evaluation of the field gradient

With the measurements done inside the BSC, it is possible to determine the gradient of a B-field applied outside, or, at least, to have an evaluation of it. In order to do this task, there is some steps to do before. First, we must calculate the field produced by the coil without the presence of the magnetometer. After, we must isolate the gradient due to the BSC; this signifies that we must remove the part of the gradient due to the coil we just calculated. At last, we compare the different plots obtained previously in order to determine/evaluate the field gradient.

5.2.1 Horizontal gradient

- **Calculate the field produce by the coil without the presence of the tank:**

To do that a program was made with MATLAB. It is the program called "loop.m" in the appendix. It computes the cartesian compoments of magnetic field due to a current I in a loop of a radius a at the point x,y,z. This program is based on the following equations that describes the magnetic induction for a circular current loop. An interested reader could find references in [2].

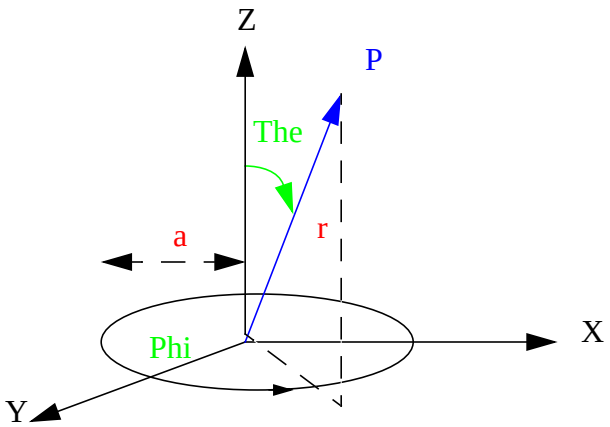

In polar coordinate, the radial compoment of the magnetic field could be written as:

$$B_r = \frac{2\pi Ia}{cr}\sum_{n=0}^{\infty}\frac{(-1)^n(2n-1)!!}{2^n n!}\cdot\begin{Bmatrix}\dfrac{r^{2n-1}}{a^{2n+2}}\\[2ex]\dfrac{a^{2n-1}}{r^{2n+2}}\end{Bmatrix}P_{2n+1}(\cos\theta)$$

Where *P* represents a Legendre polynomial. The angular compoment is similarly:

$$B_\theta = \left(-\frac{\pi Ia^2}{c}\right)\sum_{n=0}^{\infty}\frac{(-1)^n(2n-1)!!}{2^n(n+1)!}\begin{Bmatrix}-\left(\dfrac{2n+2}{2n+1}\right)\cdot\dfrac{1}{a^3}\cdot\left(\dfrac{r}{a}\right)^{2n}\\[2ex]\dfrac{1}{r^3}\cdot\left(\dfrac{a}{r}\right)^{2n}\end{Bmatrix}\cdot P^1_{2n+1}(\cos\theta)$$

The upper line hold for $r<a$, and the lower line for $r>a$ (with a the radius of the coil). It is easy to have the cartesian coordinate, we just applies the following formula:

$$B_x = B_r\sin\theta\cos\varphi + B_\theta\cos\theta\cos\varphi$$
$$B_y = B_r\sin\theta\sin\varphi + B_\theta\cos\theta\sin\varphi$$
$$B_z = B_r\cos\theta - B_\theta\sin\varphi$$

- **Field gradient due to the BSC:**

After calculating this field, we print on the same plot and at the same scale all the measurements that are on the same height, e.g. 177.5 cm. We subtract this calculated field to the values of the plot obtained. We are allowed to do that because the field gener-

ated by the coil without the presence of the BSC (the calculated field) is independant of the frequency, it is only function of the position. Then we obtain the following plot:

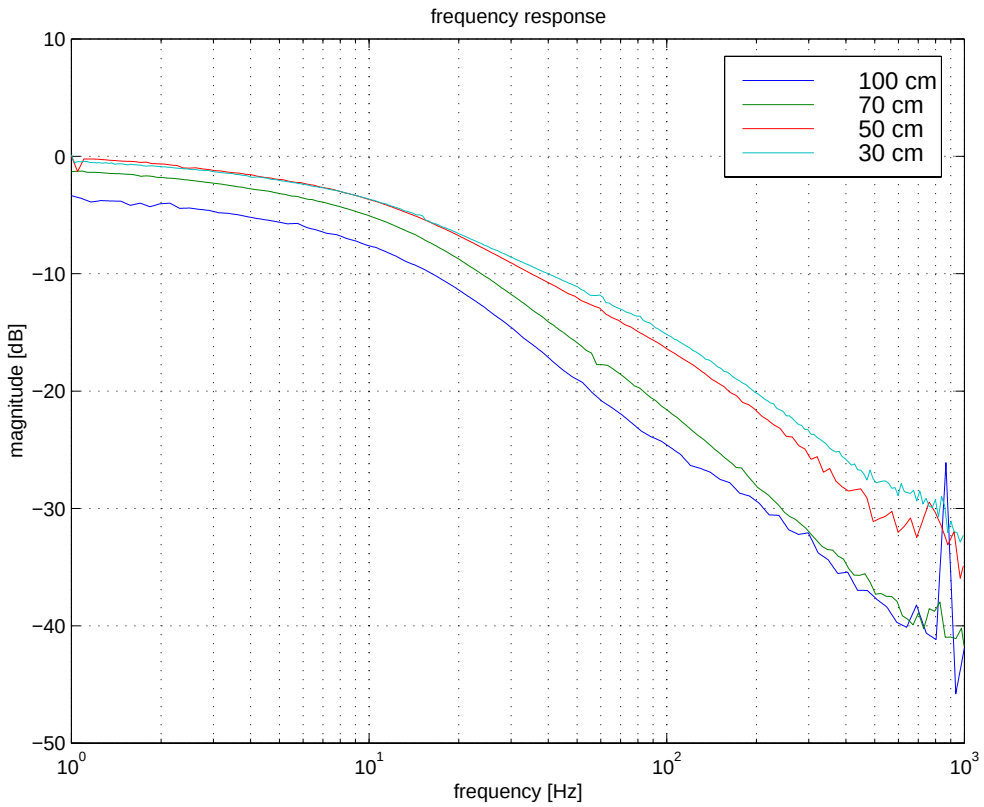

Each plot was obtained at a certain distance from the center of the BSC. This distance is represented on the upper right corner. 30 cm means that this plot was obtained at 30 cm from the center of the BSC

Now, we have a plot with only the horizonthal magnetic gradient due to the effect of the BSC. If there was no gradient caused by the tank, all the plot would be spperposed, and it is not the case here.

- **Comparaison of plots in order to determine the field gradient:**

To have a numerical value of the gradient with respect to the frequency, we must compare the previous plot. But we can not do that as we want; it is useless to compare certains plots, because the gradient has only a sense between two consecutives points, for a given height. So, I will calculate the gradient between the following plot: 10-11, 2-10, 3-2 and 3-11 (the last one is to have an idea of the gradient between the extremal points). Then we obtain the following plots; a legend is on the top of each plot.

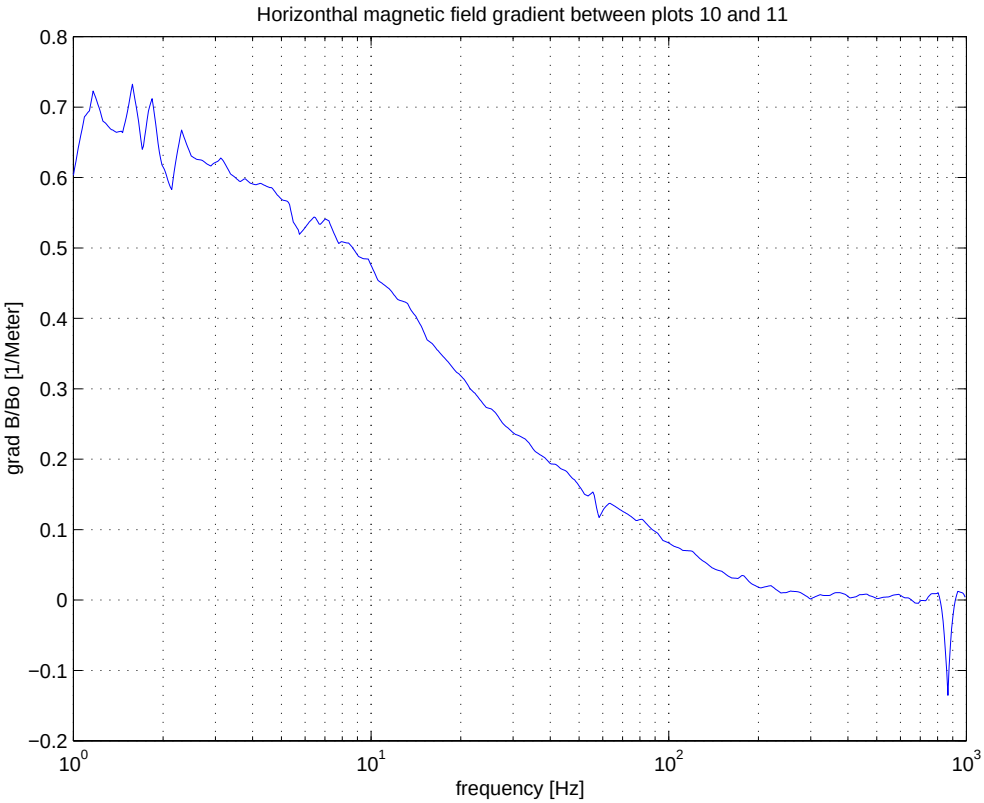
Horizonthal magnetic field gradient between plots 10 and 11
grad B/Bo [1/Meter]
frequency [Hz]
0.8
0.7
0.6
0.5
0.4
0.3
0.2
0.1
0
−0.1
−0.2
10^0
10^1
10^2
10^3

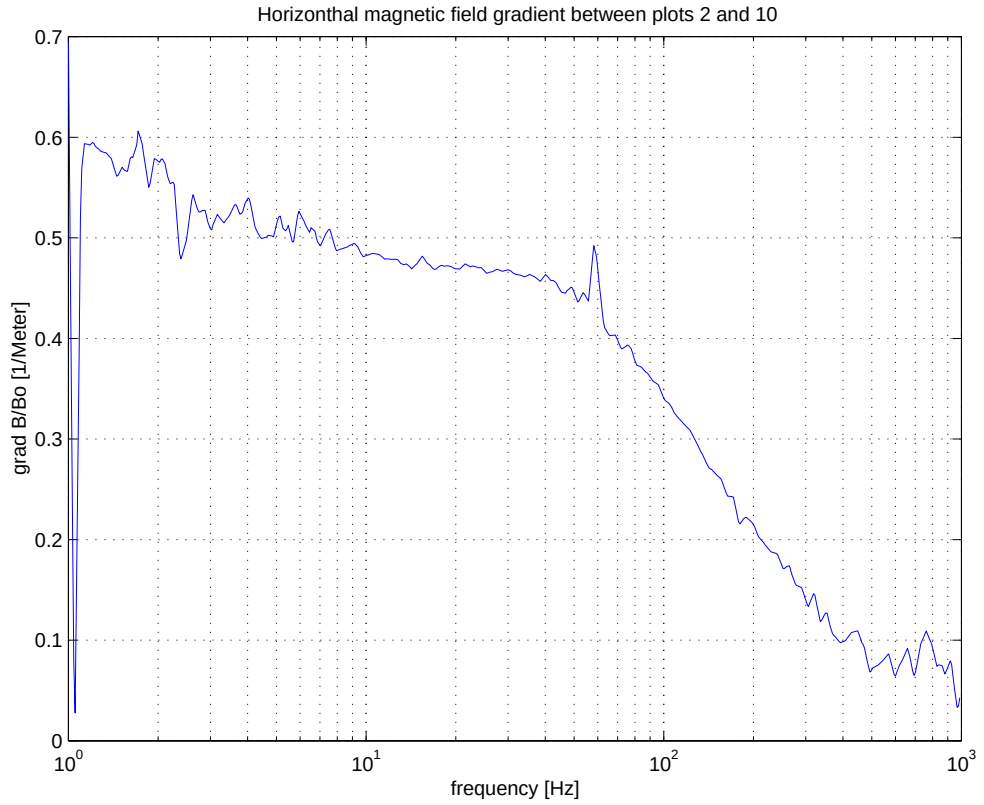
Horizonthal magnetic field gradient between plots 2 and 10
grad B/Bo [1/Meter]
frequency [Hz]
0.7
0.6
0.5
0.4
0.3
0.2
0.1
0
10^0
10^1
10^2
10^3

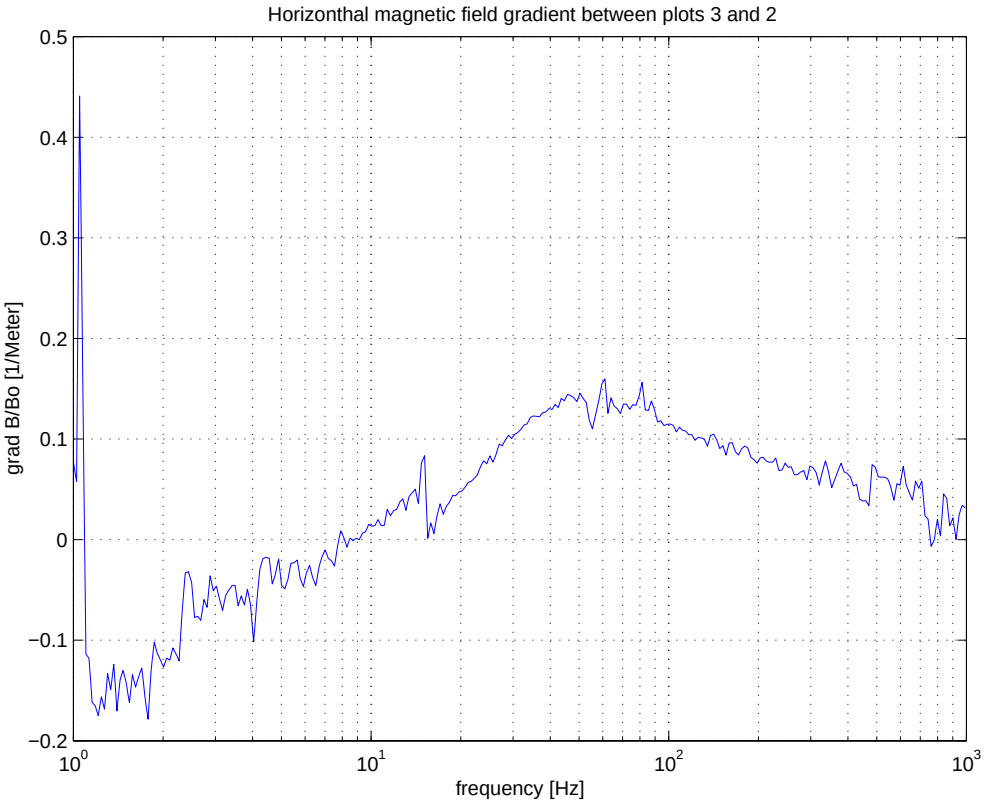
Horizonthal magnetic field gradient between plots 3 and 2
grad B/Bo [1/Meter]
frequency [Hz]
0.5
0.4
0.3
0.2
0.1
0
−0.1
−0.2
10^0
10^1
10^2
10^3

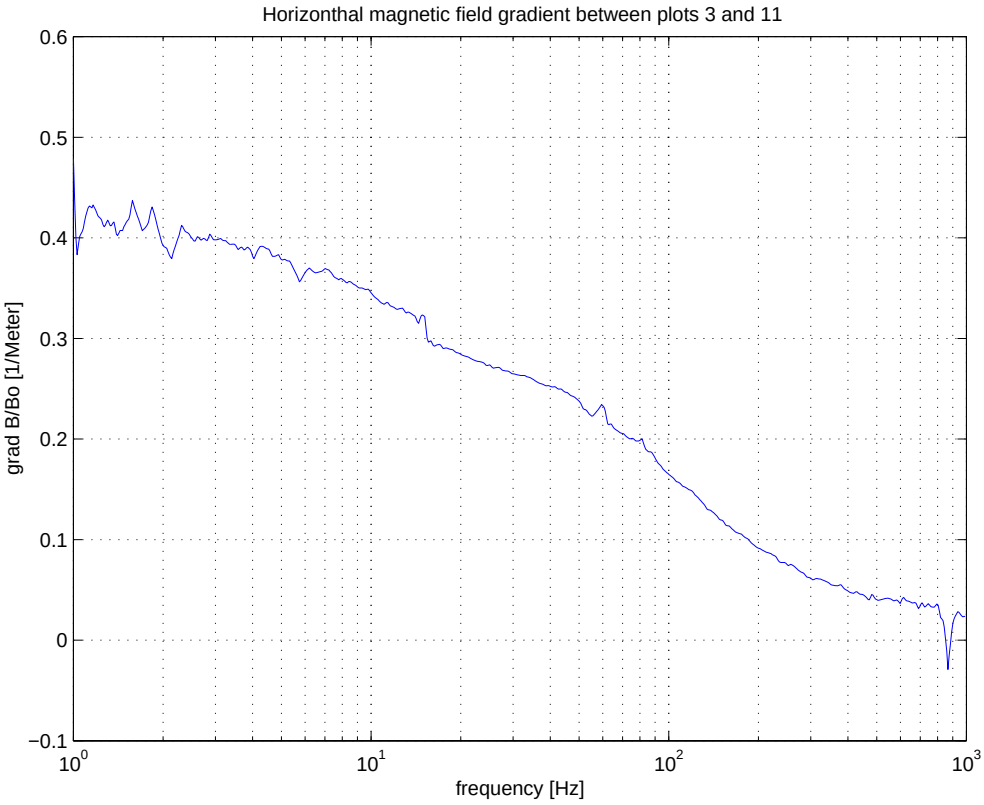
Horizonthal magnetic field gradient between plots 3 and 11
grad B/Bo [1/Meter]
frequency [Hz]
0.6
0.5
0.4
0.3
0.2
0.1
0
−0.1
10^0
10^1
10^2
10^3

It is not useless to give an explanation of the scale used on the *y* axis. *grad* B/B_0 signifies that we have took an outside field of 1 Tesla (B_0), and if a field with another magnitude is applied, we just have to multiply the value on the *y* axis by the value of this field.

As we have seen, the sensitivity of LIGO is around 100 Hz, so it is at this frequency that we are interested by the magnetic gradient. The value of the gradients at 100 Hz are:

$$grad\frac{B}{B_0} = 0.0833m^{-1} \text{ for plots 10-11.}$$

$$grad\frac{B}{B_0} = 0.3457m^{-1} \text{ for plots 2-10.}$$

$$grad\frac{B}{B_0} = 0.1153m^{-1} \text{ for plots 3-2.}$$

$$grad\frac{B}{B_0} = 0.1692m^{-1} \text{ for plots 3-11.}$$

It is exactly the kind of results we expected. If we plot the theoretical intensity of the B-field produce by a coil with respect to the distance away from the center of the coil, at the high z = 177.5 cm, we obtain:

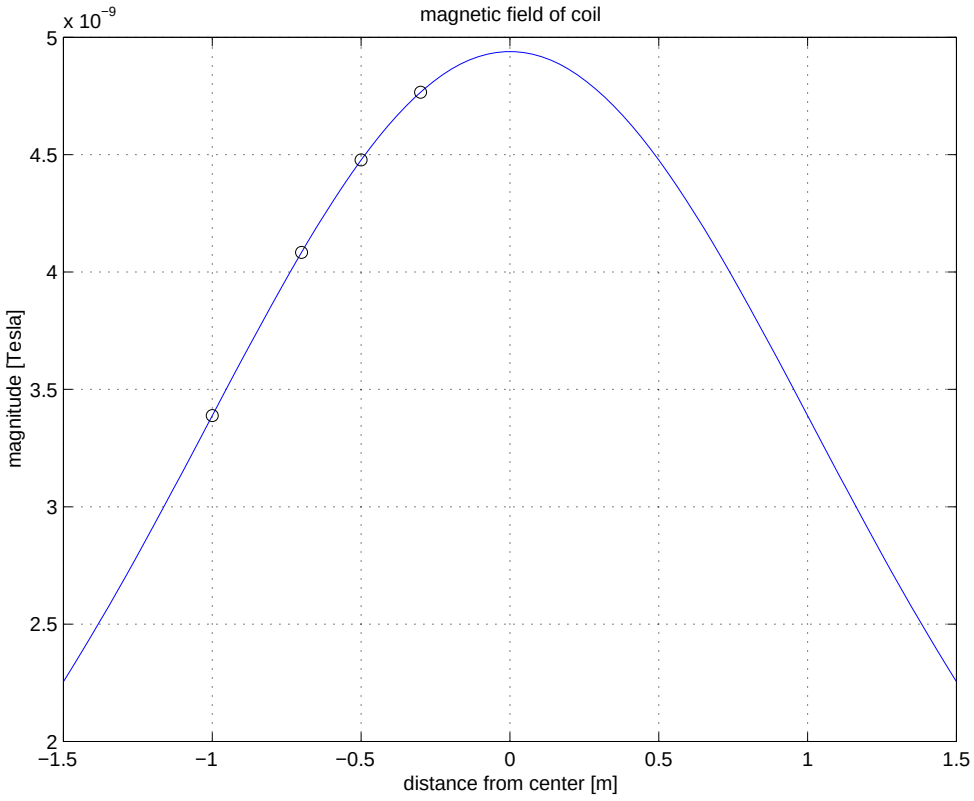

The gradient represents the derivative of this plot. So for the plot of the gradient with respect to the distance away from the center of the tank, we expect (in an ideal case) that the gradient will be zero at the center of the BSC, presents a maximum ont the left side of the plot (x < 0) and a minimum on the right side (x > 0). Unfortunately I don't have enough points to draw something, but you see that the values of the points I have for the gradient match the ideal case.

5.2.2 Vertical gradient

We do exactly the same operation, but we take three measurements at the same *x* and with different height. We obtain the following plot, at x = 70 cm from the center.

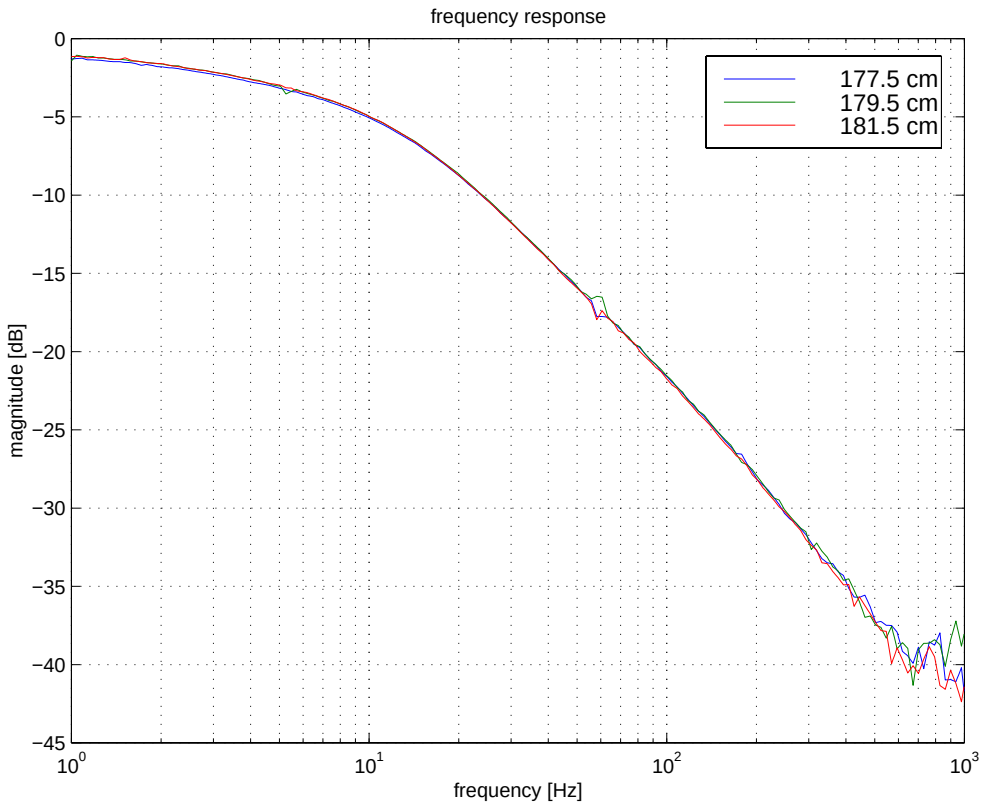

The three plot are superposed, it signifies that there is no gradient between them. It is a good result, but we must consider that the distance between two different high is very close (0.02 meters), so it is normal to not find a significant variation fo the gradient.

I do not do this work for the other plot, because it will show us the same result, e.g. that there is no significant vertical gradient with the range used.

The anomaly on the plot at 60 Hz is due to the magnetic field created by the power line.

6. Conclusion

The LIGO gravitational wave detector must detect variations of distance of 10^{-19}, it is smaller than the radius of a proton, and it is easy to guess that there is a lot of potential source of “noise”. One of them could be the variation of magnetic field. My work here was to characterize the magnetic field gradient induces by the tank, and determine if it could cause a variation of position of the test mass.

After measuring the field inside the tank, I have used some programs to analyze these data and determine the field gradient. However, the measurements that I made could be ameliorated as follows:

- In addition to putting the coil under the BSC, it will be a good idea to put it in parallel with the tank. The reasons are that the eddy current will have a more difficult geometry to follow, so the attenuation at high frequencies will be less than the one obtained in our case. The Earth magnetic field is directed, at our scale, quasi parallel to the Earth’s surface. And the last one is the more evident, there is no kind of magnetic field pertubations that will come from under the tank.

- The number of measurements I have took was not enough. We need more measurements to correctly characterize the field gradient inside the chamber.

Fortunately my work was not useless, it gives a first approach of the kind of magnetic field gradient we can expect inside the chamber. When the theoretical gradient that could pertubates the magnet will be know, it will be possible to determine if we can be worried about the magnetic noise. A possible way to determine this gradient could be to do measurements with a fake test mass a real magnets using a coil or something that generate a field that we could precisely know for a given position. All of this proposition could be done in a further work.

7. Appendix

7.1 Program “plotmag.m”

```
file = 'outside.data';                          % data file
data = load(file);                              % load data file


x = data(:,1);                                  % coordinate [feet]
y = 2 * data(:,2);
z = data(:,3);

Bx = data(:,6);                                 % magnetic field [gauss]
By = -data(:,4);
Bz = -data(:,5);

x = x * 12 * 2.54 / 1e2;                        % convert to meter
y = y * 12 * 2.54 / 1e2;
z = z * 12 * 2.54 / 1e2;

Bx = Bx  * 1e-5;                                % convert to tesla
By = By  * 1e-5;
Bz = Bz  * 1e-5;

B = sqrt(Bx.^2 + By.^2 + Bz.^2);                % magnitude of field


res = 0.05;                                     % interpolation
grid xi = min(x)-res : res : max(x)+res;
yi = min(y)-res : res : max(y)+res;
[XI,YI] = meshgrid(xi,yi);

BI = griddata(x,y,B,XI,YI);                     % interpolated field


% mesh(XI,YI,BI);
% plot interpolated field
% hold on
% plot original data
% plot3(x,y,B,'k*');
% hold off;
% title('magnetic field magnitude');
% xlabel('X [meters]');
% ylabel('Y [meters]');
```

```
% zlabel('magnetic field magnitude [tesla]');

contour(XI,YI,BI,30);
hold on;
plot(x,y,'k.');
xlabel('X [meters]');
ylabel('Y [meters]');
title('magnetic field magnitude');
```

The inputs of this program are the file called “outside.data”, which contains six columns. Three of these columns contain the components of the B-field, and the other three ones contain the coordinates of the points where the B-field was taken. One of the coordinate is constant because the measurements were done in only two dimensions, but the function used in MATLAB need to have six matrix elements. As we want to have a map in three dimensions, and as there is a couple of points which are missing (it was not possible to acquire data where is the BSC), a program that interpolates this points was made using a function of MATLAB.

7.2 Program “loop.m”

```
function [Bx, By, Bz] = loop(x, y, z, a, i)
% [Bx, By, Bz] = loop(x, y, z, a, i)
%
% compute cartesian components of magnetic field due to
% a current i flowing in a loop of radius a at the point
% x, y, z.
%

N = 10;

mu = 4 * pi * 1e-7;

r = sqrt(x.^2 + y.^2 + z.^2);
theta = atan2(sqrt(x.^2 + y.^2), z);
phi = atan2(y, x);

Br = 0;
Btheta = 0;

for n = 0 : N,
   P = legendre(2*n+1,cos(theta));
   tmp(r<a) = (-1)^n * prod(2*n+1:-2:1) * r(r<a).^(2*n) / (2^n *
                                                    a^(2*n+1));
   tmp(r>a) = (-1)^n * prod(2*n+1:-2:1) * a^(2*n+2) ./ (2^n *
                                                  r(r>a).^(2*n+3));
   tmp(r==a) = (-1)^n * prod(2*n+1:-2:1) ./ (2^n * a);
   Br = Br + tmp .* P(1,:) / prod(1:n);
```

```
   dBtheta = tmp .* P(2,:) / prod(1:n+1);
   dBtheta(r<a) = dBtheta(r<a) * (2*n+2) / (2*n+1);
   Btheta = Btheta + dBtheta;
   end

Br = Br * mu * i / 2;
Btheta = Btheta * mu * i / 4;

Bx = Br .* sin(theta) .* cos(phi) + Btheta .* cos(theta) .* cos(phi);
By = Br .* sin(theta) .* sin(phi) + Btheta .* cos(theta) .* sin(phi);
Bz = Br .* cos(theta) - Btheta .* sin(theta);
```

This program allow us to calculate a B-field generated by a coil of radius a. The number of iteration is 10, because after the value does not differ significantely. The formula from [2] uses polar coordinate and we have measurements in cartesian coordinate, so we make the conversion between them. We use an iterative loop to calculate the value of the field, and then we convert the polar value of the B-field into cartesian value.

7.3 Program “compare_adj.m”

```
load MEAS11.MAT
H11 = o2i1(o2i1x<=1e3);
f11 = o2i1x(o2i1x<=1e3);
dB11 = 20 * log10(abs(H11));
dB11 = dB11 + 28.32;
B11 = 10.^(dB11/20);

load MEAS10.MAT
H10 = o2i1(o2i1x<=1e3);
f10 = o2i1x(o2i1x<=1e3);
dB10 = 20 * log10(abs(H10));
dB10 = dB10 + 26.52;
B10 = 10.^(dB10/20);

load MEAS2.MAT
H2 = o2i1(o2i1x<=1e3);
f2 = o2i1x(o2i1x<=1e3);
dB2 = 20 * log10(abs(H2));
dB2 = dB2 + 25.60;
B2 = 10.^(dB2/20);

load MEAS3.MAT
H3 = o2i1(o2i1x<=1e3);
f3 = o2i1x(o2i1x<=1e3);
dB3 = 20 * log10(abs(H3));
```

```
dB3 = dB3 + 24.96;
B3 = 10.^(dB3/20);



B3 = interp1q(f3, B3, f11);
gradB = (B3-B11)/0.7;


clf;
semilogx(f11, gradB);
grid;
xlabel('frequency [Hz]');
ylabel('grad B/Bo [1/Meter]');
title('Horizonthal magnetic field gradient between plots 3 and 11');
```

This program load all the measurements that are at the high of 177.5 cm. It soustracts the value of the theoretical field found with the program "loop.m".

During the acquisition, I change the range of frequencies, so the interval of measurements was not the same. In order to compare things that coresponds to a given frequency, this program makes an interpolationof the plot to have a field value at all frequencies. At last, to find the gradient, the program soustract the value of two plots and divided this value by the distance between the points where these plots were made, and that for all frequencies.

7.4 Bibliography

[1] : Hermann A. Haus, James R. Melcher, " *Electromagnetic Fields and Energy* ", Prentice Hall (1989).

[2] : John D. Jackson, " *Classical Electrodynamics* ", John Wiley & sons (1962).

[3] : Sanichiro Yoshida, Rana Adhikari, David Reitze, " *Influence of the stray magnetic field generated by the faraday isolator on SOS mirror actuators* ", California Institute of Technology and Massachusetts Institute of Technology (1996).

[4] : Seiki Kawamura, Janeen Hazel, Mark Barton, " *Large Optics Suspension Final Design (Mechanical System)* ", California Institute of Technology and Massachusetts Institute of Technology (1997).

[5] : Kip S. Thorne, " *Gravitation Radiation* ", in " *300 Years of Gravitation* ", S.W. Hawking and W. Israel, Cambridge U, Press (1987).

[6] : Paul R. Saulson, " *Fundamentals of Interferometric Gravitational Wave Detectors* ", World Scientific (1994).

7.5 Clean room and BSC picture